# Radar Observations of Spacecraft in Lunar Orbit

By Marina BROZOVIĆ,[1)] Ryan S. PARK,[1)] Joseph G. MCMICHAEL,[1)] Jon D. GIORGINI,[1)] Martin A. SLADE,[1)] David S. BERRY,[1)] Joseph S. JAO,[1)] Frank D. GHIGO,[2)] Patrick A. TAYLOR,[3)] and Edgard RIVERA-VALENTÍN[3)]

[1)] *Jet Propulsion Laboratory/California Institute of Technology, Pasadena, California, USA*
[2)] *Green Bank Observatory, Green Bank, West Virginia, USA*
[3)] *Arecibo Observatory/Universities Space Research Association, Arecibo, Puerto Rico, USA*

(Received June 21, 2017)

Radar measurements of relative position and velocity via round-trip time-delay and the Doppler frequency-shift of the return echo provide powerful constraints for orbit determination. We report the first use of ground-based Goldstone and Arecibo radars to detect and determine the trajectories of spacecraft in lunar orbit, using techniques developed for radar observations of near-Earth asteroids (NEAs) (https://echo.jpl.nasa.gov/). Maintaining the orbital knowledge of old spacecraft that are still orbiting the Moon is important because these spacecraft pose a potential impact hazard for future human and robotic missions.

**Key Words:** Planetary radar, spacecraft, radar astrometry, orbit determination

## 1. Introduction

The Goldstone Solar System Radar (GSSR) and Arecibo Observatory radar are powerful instruments that are used to study solar system objects such as asteroids,[1-3)] comets,[4)] terrestrial planets,[5-7)] moons of Jupiter,[8)] and rings of Saturn.[9)] GSSR is a 70-m diameter antenna (DSS-14) that has 450 kW output power and works in X-band (8560 MHz, 3.5 cm). Arecibo is a 305-m diameter antenna that has 1 MW output power and works in S-band (2380 MHz). Arecibo is 20 times more sensitive than Goldstone, but its pointing is limited to 20° of zenith. DSS-14 antenna is a fully steerable and it covers 80% of sky (everything north of 35°S in declination). Goldstone and Arecibo are currently the only radars in the world capable of detecting meter(s)-sized objects at one lunar distance and beyond. Radar tracking is different than a spacecraft radiometric tracking because the spacecraft does not need to have a functioning transponder that re-transmits a received signal at an offset frequency.

Arecibo and Goldstone were used to recover the Solar and Heliospheric Observatory (SOHO) in June of 1998, after the mission team lost contact with the spacecraft. SOHO is a joint project between the European Space Agency (ESA) and the National and Aeronautics Space Administration (NASA). Arecibo was used for transmitting and DSS-14 was used as the receiving antenna. In July of 1998, SOHO was found[10)] in its nominal orbit around the Earth-Sun Lagrangian point L1, approximately four lunar distances from Earth. The radar data were used to estimate SOHO's spin rate, a parameter important for alignment of the spacecraft solar panels and communication. At the time, the mission team was concerned that the spacecraft was spinning very rapidly, but radar observations showed that the spin rate was about one revolution per minute. In the following months, the mission team established contact and resumed normal operations of the spacecraft.

Following in the footsteps of the SOHO's radar recovery almost 20 years later, we used DSS-14, DSS-13, Green Bank Telescope (GBT), and Arecibo to search for two spacecraft that were no longer communicating, but for which we have indications that they are still orbiting the Moon: Chandrayaan-1 and Selenological and Engineering Explorer's (SELENE) relay satellite Ouna. We also used radar to detect NASA's active spacecraft, the Lunar Reconnaissance Orbiter (LRO).

Chandrayaan-1 is the first spacecraft built by the Indian Space Research Organization (ISRO) to orbit the Moon. The spacecraft went into lunar orbit in October 2008 and the mission ended in August 2009 when radio contact was lost. The spacecraft was left in a circular polar lunar orbit at an altitude of ~200 km with an orbital period of ~2.14 h. We used a JPL trajectory estimate[11)], made after the last Chandrayaan-1 contact in 2009, to plan our observations. The orbital uncertainties indicated that the along-track position for this spacecraft was no longer known, but that the orbital plane orientation was still well constrained.

Ouna is a small relay satellite that was originally carried by JAXA's (the Japanese Space Agency) lunar orbiter SELENE. This mission was launched in September of 2007. The main orbiter impacted the Moon at the end of the mission in June of 2010, and so did the small relay satellite (Okina or Rstar). However, the second satellite, Ouna (originally Vstar), is still orbiting the Moon according to JPL ephemerides.[12)] Ouna is in an elliptical polar lunar orbit and the orbital uncertainties show that the mean anomaly and argument of

periapsis are highly uncertain. The orbital period of Ouna is estimated to be ~2.6 h.

## 2. Methods

### 2.1 Bistatic radar

The bistatic radar experiments use one antenna for transmitting and another one for receiving. This configuration is needed when the round trip light time to the target and back is too short to switch from transmitting to receiving at a single site. For example, it takes DSS-14 ~3 s to switch to the receiving mode and the round-trip-time (RTT) for the radio signal to the Moon and back is ~2.6 s. Hence, all radar observations at one lunar distance are conducted in a bistatic mode.

The bistatic experiments can have increased sensitivity if the receiving antenna has larger surface area than the transmitting antenna. For example, receiving the transmission from DSS-14 at GBT increases the signal-to-noise ratios (SNRs) by a factor of two, and receiving at Arecibo increases the SNRs by a factor of five.[13] The additional benefit of the bistatic data is the fact that they are unconstrained in Doppler frequency resolution by the RTT time. This is important when we are trying to resolve an echo that has very narrow bandwidth in Doppler frequency, such is a case with a spacecraft echo.

### 2.2. Radar SNRs

The prerequisite for radar observations is that the target reflects enough of the transmitted signal back. The SNRs are calculated based on the monostatic radar equation[1,14] for an idealized, spherical target:

$$SNR \propto \left(\frac{P_{tx} G^2 \lambda^{3/2}}{T}\right)_{system} \left(\frac{\hat{\sigma} D^{3/2} P^{1/2}}{R^4}\right)_{target} \sqrt{\tau} \qquad (1)$$

The SNRs depend on both the system and target parameters. The system parameters are the transmit power, $P_{tx}$, the antenna gain, G, the wavelength, $\lambda$, and the temperature of the receiver, T. The target parameters are the radar albedo, $\hat{\sigma}$, the target's diameter, D, the target's rotation period, P, and distance between the observer and the target, R. $\tau$ is the time during which we collect/integrate the signal on the receiving end. For objects with well-determined orbits, we can integrate the data for hours at a time, but for a spacecraft with an unknown orbit that sweeps though the radar beam in a matter of minutes with unknown delay-Doppler and unknown rates, we need a strong echo that can become visible within several seconds of integration time.

Table 1 shows the SNRs for LRO, Chandrayaan-1, and Ouna for a bistatic experiment where DSS-14 is transmitting and GBT is receiving. These estimates should be regarded as "order-of-magnitude" SNRs, because we made some assumptions about the spacecraft average diameters and rotation periods. In addition, the SNRs assume that the echo is not smearing (and diminishing) because of the unknown orbit.

Rotation period is also important for the Doppler broadening (or the bandwidth) of the target's echo:

$$B = \frac{4\pi D}{\lambda P}\cos(\delta) \qquad (2)$$

where B is the bandwidth and $\delta$ is the subradar latitude.

The LRO is a large spacecraft, 3.9 × 2.7 × 2.6 m in size and we assumed that its rotation period is synchronous with the orbital period of ~2 h. This spin state allows the LRO's instruments to be continuously pointed toward the lunar surface. Table 1 shows that the LRO should be easily detectable using DSS-14 and the GBT. From Eq. (2), we estimated that the LRO's bandwidth due to its intrinsic spin rate should be ~0.13 Hz in X-band.

Chandrayaan-1 is roughly cubical, approximately 1.5 m in each dimension and it has an extended solar panel with dimensions of 2.15 × 1.8 m. We used an approximate diameter of 2 m and calculated SNRs for a range of rotation periods from 0.1–2 h. Chandrayaan-1 was once also rotating synchronously with respect to its orbit like the LRO, but we do not know if that is still the case. The lower bound on the rotation period, 0.1 h, has the purpose of establishing the conservative SNRs. The SNRs in Table 1 are still very strong and imply that Chandrayaan-1 detection is possible.

Ouna has dimensions 1.0 × 1.0 × 0.65 m and it does not have an extendable solar panel like Chandrayaan-1. We assumed that its overall diameter is ~0.7 m and that is has a rotation period from 0.1–2 h. The SNRs are significantly lower than for the LRO and Chandrayaan-1.

Table 1. Spacecraft SNRs at one lunar distance for the DSS-14 and GBT bistatic experiment. The SNRs were calculated based on Eq. (1). The system parameters are: $P_{tx}$ = 450 kW, G = 0.94 K/Jy, $\lambda$ = 3.5 cm, and $T_{GBT}$ = 23 K. The round-trip-time at one lunar distance is ~2.6 s.

| Spacecraft | D(m) | P(h) | SNRs/RTT |
|---|---|---|---|
| LRO | 2.6 | 2.0 | ~1700 |
| Chandrayaan-1 | 2.0 | 0.1-2.0 | ~260–1200 |
| Ouna | 0.7 | 0.1-2.0 | ~60–240 |

### 2.3 Antennas beam widths

The 3 dB beam width, or the half-power beam width, is the region of the antenna's main lobe, measured as an angle, where the relative power remains at or above 50% of the peak power. We show the beam widths for the antennas used in spacecraft detections in Fig. 1. The DSS-14 and Arecibo transmitters have roughly the same 3 dB beam widths, 108″ and 120″ respectively. The receiving beams can vary by an order of magnitude, 30″–312″, which translates into ~60–580 km at one lunar distance. The spacecraft needs to be "lit" by the transmitting beam to be detected, but sometimes it can

even be in the side-lobes, and still be detectable assuming that the receiving beam is wide enough and that the SNRs are strong.

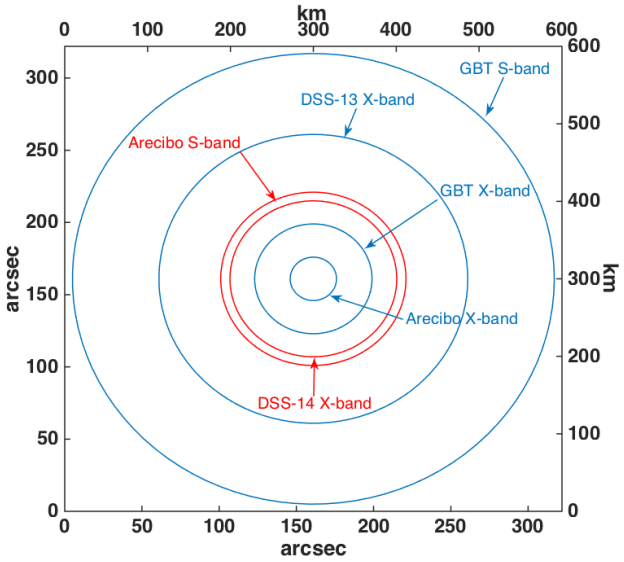


Fig. 1. Sizes of the 3 dB beam widths for DSS-14, DSS-13, Arecibo, and the GBT. The red circles represent the transmitting antennas beams and the blue are the receiving antennas beams.

### 2.3. Radar observations

We observed lunar spacecraft with radar on five days from July 2 to September 23, 2016. Table 2 lists the observing times, antennas used for transmitting and receiving, and the spacecraft detected. We exercised all available antennas configurations for this experiment and the spacecraft were detected in both X- and S- bands. The LRO was detected five times, Chandrayaan-1 nine times, and we have a candidate detection of Ouna.

Table 2. Masterlog of radar observations in 2016. The table lists start and stop times, transmitting (Tx) and receiving (Rcv) antennas, frequency band, and spacecraft detected. Numbers ×2, ×3, ×4 denote how many times the spacecraft was detected on each day.

| Date UTC | Start-Stop hh:mm-hh:mm | Tx | Rcv | Band | Detected |
|---|---|---|---|---|---|
| 07-02 | 13:00–17:30 | DSS-14 | GBT | X | LRO×3, Ch-1×2 |
| 07-03 | 14:40–18:02 | DSS-14 | GBT | X | LRO, Ch-1×4 |
| 07-31 | 12:35–15:55 | DSS-14 | GBT | X | Ch-1, LRO |
| | | | DSS-13 | X | Ch-1, LRO |
| 08-26 | 10:04–12:53 | Arecibo | GBT | S | Ch-1, Ouna? |
| 09-23 | 08:58–11:47 | DSS-14 | Arecibo | X | Ch-1 |

On July 31, we used two antennas to receive in parallel: GBT and DSS-13. The 34-m antenna DSS-13 at Goldstone is relatively easy to schedule as the receiving station, but it is only about 1/8 as sensitive[13] as the GBT. Table 1 indicates that the SNRs for the LRO and Chandrayaan-1 were predicted to be sufficient for detection even at reduced rates. On July 31, the DSS-13 detections were very weak, but consistent in timing and Doppler frequency with much stronger GBT detections. DSS-13 is a valuable asset for radar observations of spacecraft that are strong radar targets and that have well known orbits, but a larger antenna is needed for a spacecraft search.

We used Arecibo to transmit and GBT to receive on August 26. This configuration is about a factor of 2.5 more sensitive[13] than the DSS-14 and GBT and it also has the widest beam widths (Fig. 1). This is an ideal combination to search for a small spacecraft with highly uncertain orbit such as is the case for Ouna. Arecibo was operating at only 400 kW, or 40% of the full power during our track, so the SNRs were comparable to the SNRs estimated in Table 1.

The last track on September 23 occurred during an island-wide power outage in Puerto Rico and Arecibo observatory was running on local generators. The entire track between the DSS-14 and Arecibo was coordinated via a land-line phone. The Chandrayaan-1 orbit was well known at this time, so we were able to obtain detection. This configuration of the antennas, with DSS-14 transmitting and Arecibo receiving is potentially very powerful, a factor of 2.5 more sensitive than DSS-14 and the GBT. However, the beam width for Arecibo in the X-band is very narrow, only 60 km, so this is not an ideal antenna combination when searching for a lost spacecraft.

### 2.4. Radar data

We transmitted a circularly polarized continuous wave (CW) at a carrier frequency plus a nominal +1 kHz transmit offset. This offset was used as a cross-check of a positive Doppler frequency direction. The received spacecraft echo had its frequency shifted with respect to reference frequency due to the spacecraft motion relative to the transmitter and receiver. The received signal was recorded in a form of complex voltages that have real and imaginary parts corresponding to the in-phase (I) and quadrature-phase (Q). The voltages were sampled at rates of 2 MHz, 6.25 MHz, or 10 MHz depending on the receiving system.

We used Discrete Fourier Transform (DFT) to obtain a power spectrum with respect to Doppler frequencies. Ideally, the Doppler shifts are removed based on the predicted motion of the spacecraft at each time step, and the processed echo is centered at the offset frequency (+1 kHz). This is a standard procedure during asteroid tracks, [15] but for the case of "lost" spacecraft, we did not know the orbital Doppler shifts a-priori. Instead, we had to search for the spacecraft echo in uncompensated Doppler frequencies, which for a lunar orbiting spacecraft translates into Doppler shifts of tens of thousands or hundreds of thousands of Hz with respect to the transmit frequency.

Once the spacecraft echo was detected, the Doppler frequency measurements were used to estimate new orbital solution. The data were then re-processed with Doppler compensation, and the spacecraft signal got amplified. This

procedure can be described as “shift-and-stack in frequency domain”. Any residual Doppler shifts that were not removed by the initial orbital solution were used to refine the astrometry, and this resulted in another orbital update. In only two steps, the data weights that we assigned to the Doppler frequency measurements decreased from over 100 Hz to less than 5 Hz. At X-band, 5 Hz uncertainty in Doppler frequency is equivalent to 0.09 m/s uncertainty in the line-of-sight velocity.

On July 3, we also transmitted a signal that was modulated in amplitude via a pseudo-random binary code, so called “long code”.[16] This type of code carries information about the Doppler frequency shift and the time-delay (or range) of the target. The time-delay resolution (or baud) was 0.5 μs or 75 m. We detected Chandrayaan-1 twice, once above the south lunar pole and once above the north lunar pole. This was the first radar ranging detection of a spacecraft at lunar distances. The SOHO spacecraft was only detected in Doppler frequency in 1998. The long code detection of a spacecraft depends on having at least some kind of a starting orbital solution. The echo is otherwise lost in both Doppler (frequency) and range (delay timing) and the signal strength is smeared in two dimensions as opposed to only in Doppler frequency.

### 2.5. Orbital fit

The radar astrometry of Chandrayaan-1 was statistically fit using JPL’s Mission-analysis, Operations, and Navigation Toolkit Environment (Monte)[17] software set, which has been used to reconstruct the orbits of numerous space missions,[18,19] including NASA’s Gravity Recovery And Interior Laboratory (GRAIL). We used a dynamical model similar to what was used for reconstructing the orbits of GRAIL probes, which includes N-body dynamics, a degree and order 900 lunar gravity field, and solar radiation pressure.[20-22]

## 3. Results

### 3.1. Detections of LRO

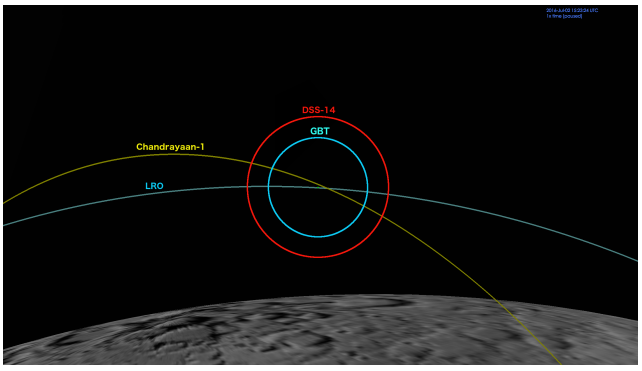


Fig. 2. Spacecraft orbital geometry during July 2 observations. The green dot marks the pointing (80°E, 83°N, 165 km) for both DSS-14 and the GBT antennas. The red circle is the DSS-14 3 dB beam width, ~108″ and the cyan circle is the GBT 76″ beam width. The yellow and light blue are Chandrayaan-1 and LRO orbital trajectories with respect to radar line of sight.

The LRO is an active mission for which we have very precise estimates of its location. The LRO management was notified about our planned experiments and we had their approval to radiate at the spacecraft.

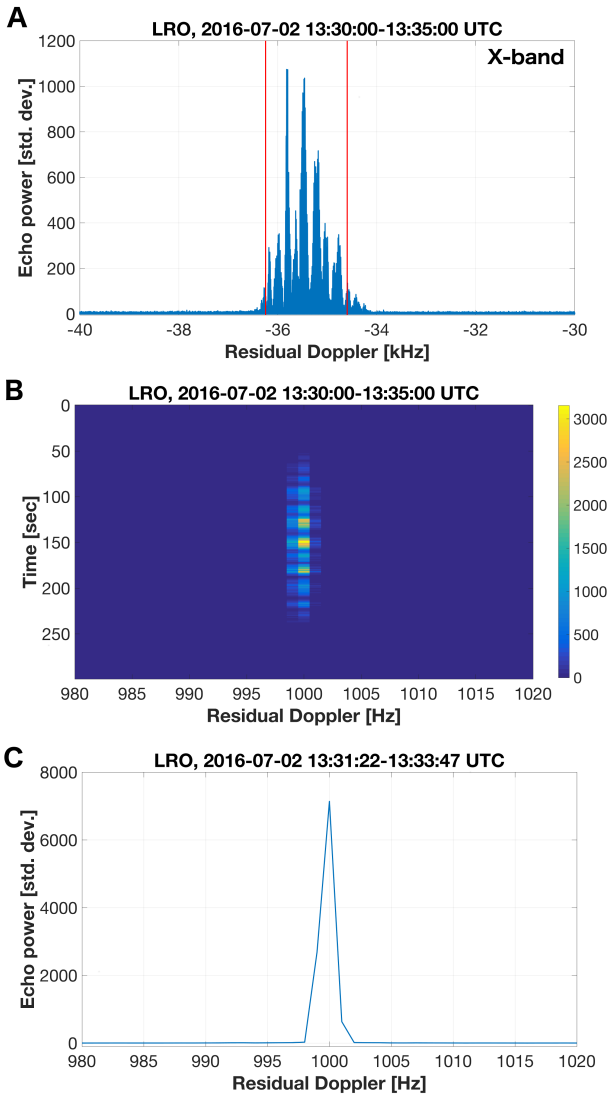


Fig. 3. First detection of the LRO on July 2 with DSS-14 and the GBT. (A) Doppler frequencies were not corrected for the relative motion of the transmitter, target, and receiver. The data were summed for 1 s and processed with 1 Hz resolution. The red lines mark the predicted 3 dB DSS-14 beam crossing. The echo power is in units of standard deviation above the noise level. (B) LRO echo power in time and Doppler frequency after orbital Doppler frequencies were removed. The echo is centered at the transmit frequency offset of +1 kHz. (C) LRO echo power obtained from a sum of all the data within the red lines and with the orbital Doppler frequencies removed.

We successfully detected LRO on July 2, 3, and 31 according to the orbital predicts. Figure 2 visualizes the orbital geometry for the LRO during the July 2 track and Fig. 3 shows the first radar detection. Figure 3A shows the original spacecraft echo prior to any Doppler compensation. The echo was detected at the correct range of Doppler frequencies, −34 to −36 kHz, it had the correct duration (~2.5 minutes) as the

spacecraft entered and exited the radar beam, and it also had the expected SNRs (Table 1). The echo in Fig. 3A displays a typical "glinty" behavior of a spacecraft echo, similar to what was reported for SOHO. Spacecraft generally have large flat faces (e.g. solar panels) that can bounce back the radar beam very efficiently when they are perpendicular to the radar line of sight, but they can also go into a "stealth" mode when the flat surfaces are parallel. Consequently, it is expected for spacecraft echoes to show large changes in the SNRs.

Figures 3B and 3C show the LRO radar echo after the orbital Doppler compensation. Figure 3B shows a time lapse of the echo power strength during 5 minutes of observations. The echo is now centered at the offset frequency and the SNRs are stronger. Figure 3C shows the echo power strength summed during 2.5 minutes while the LRO was crossing the radar beam.

### 3.2. Detections of Chandrayaan-1

We transmitted CW for 4.5 hours on July 2. We expected to detect Chandrayaan-1 twice during this time. Figure 2 shows that July 2 had a serendipitous geometry for both the LRO and Chandrayaan-1 and that a single pointing allowed both spacecraft to cross the radar beam. LRO was used as a "test beacon" during our experiment. Its detections provided verification that we were pointed correctly and that the receiving equipment was working properly.

Chandrayaan-1 was detected twice and the echoes were 2 hours and 8 minutes apart, in agreement with the nominal orbital period. The beam-crossing times implied a shift of ~160° in the mean anomaly. Figures 4A and 4B show the detections without Doppler compensation. The spacecraft echo is weaker than the LRO echo in Fig. 3A. This is not surprising given that Chandrayaan-1 is a smaller spacecraft (Table 2). The Chandrayaan-1 echo showed the similar glinty features as the LRO.

The timings of the two detections on July 2 were used to make a rough estimates for the July 3 track. We did not have time to fit the data with an integrated orbit, but a simple approach of adjusting the mean anomaly by 160° was only ~2 minutes off in predicting the beam crossing times on July 3. On July 3, we obtained four detections of Chandrayaan-1, two with CW (Doppler-only) setup, and two with delay-Doppler images.

Figure 5 shows a delay-Doppler detection of Chandrayaan-1 as the spacecraft was passing over the South lunar pole. The image has 37.5 m/pix resolution in range, and it is the first radar ranging detection of a spacecraft at one lunar distance (note that the time-delay is consistent with the round-trip-time to the Moon and back). We did not know immediately that Chandrayaan-1 was detected this way, and it was only after we had an initial orbital solution that we were able to process the data and find the spacecraft echo.

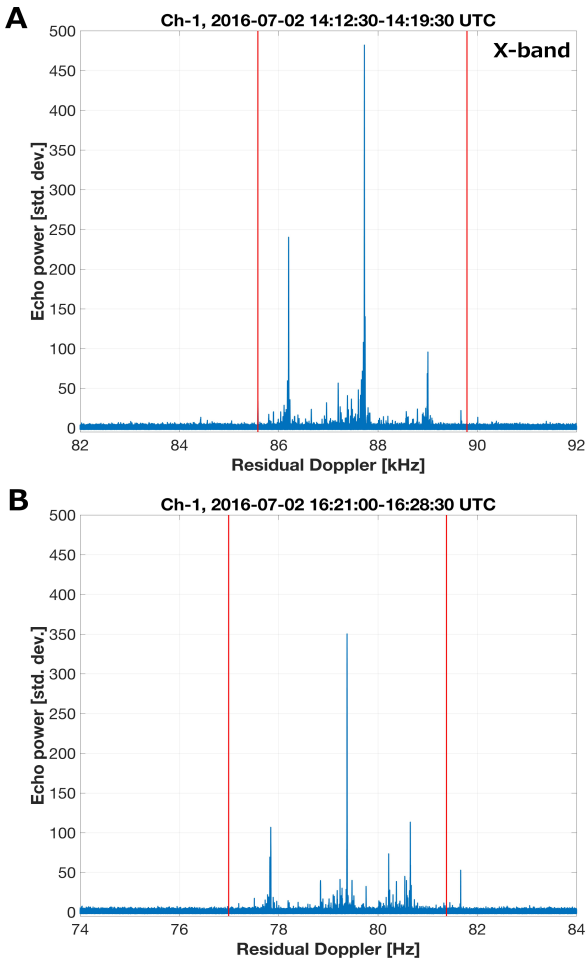


Fig. 4. Detections of Chandrayaan-1 on July 2 with DSS-14 and the GBT. Doppler frequencies were not corrected for relative motion of the transmitter, target, and receiver. The data were summed for 1 s and processed with 1 Hz resolution. The echo power is in units of standard deviation above the noise level. The red lines mark the predicted 3 dB DSS-14 beam crossing.

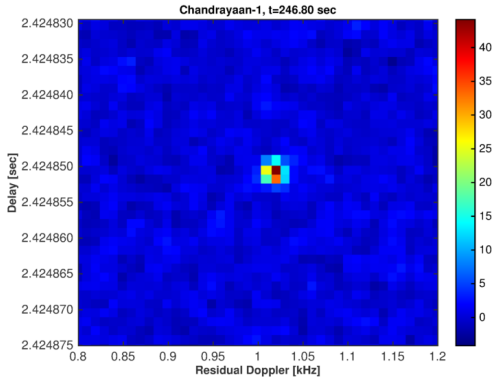


Fig. 5. Detection of Chandrayaan-1 in time-delay (range) and Doppler on July 3 with DSS-14 and the GBT. The antennas were pointed 15°W, 15°S, and 205 km above the South lunar pole. The range resolution is 75 m with 2 samples per baud, which gives an effective, but correlated resolution of 37.5 m/pix. The Doppler resolution is 10 Hz. The color scale represents the echo power in units of standard deviation above the noise level. The transmit frequency offset was +1 kHz.

### 3.3. Improved orbital fit for Chandrayaan-1

Figure 6 shows the post-fit residuals of the fitted Chandrayaan-1 radar astrometry. The residual root-mean-square (rms) is ~4 Hz, which corresponds to ~0.07 m/s in X-band. This is about a factor of 200 lower precision when compared to typical DSN-to-spacecraft two-way coherent Doppler data, but sufficiently accurate to determine the orbit of Chandrayaan-1 to better than ~1 km in position. Doppler astrometry can also be refined further.

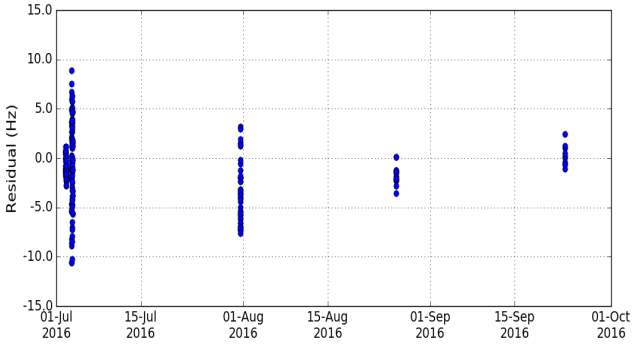


Fig. 6. Post-fit Doppler residuals for Chandrayaan-1 spacecraft. All Doppler measurements were in X-band, except for the Aug. 26 observations which were in S-band.

Figure 7 shows the mapped uncertainty of Chandrayaan-1 during the data arc, which shows that the dominating error is in the along-track direction.

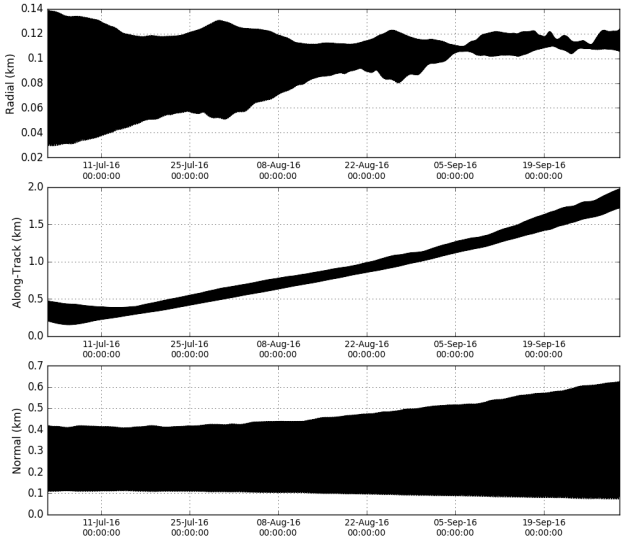


Fig. 7. Uncertainties of Chandrayaan-1's orbit in radial, along-track, and normal directions after the radar-based orbital update.

### 3.3. Candidate detection of Ouna

As a follow-up to the LRO and Chandrayaan-1 detections, we attempted to search for Ouna. This is a small spacecraft, <1 m in diameter, with large orbital uncertainties. Ouna's along-track position and argument of periapsis are not constrained with the 2010[12] orbital solution.

On August 26, we used Arecibo to transmit and Green Bank to receive. The antennas' beam widths covered only a small portion of the Ouna's orbital uncertainty space. However, we obtained candidate detection while pointed 715 km from the north lunar pole (Fig. 8). This was the expected location of Ouna's apoapsis on that day. Figure 8A shows a weak echo crossing the radar beam for about 7 minutes at Doppler frequency of −18 to −18.4 kHz in S-band. Figure 8B shows how the echo power strength changed in time and in Doppler frequency. The echo appears less glinty than the LRO and Chandrayaan-1, but this can be related to the shape of Ouna. The spacecraft is a relatively symmetric object with no solar panels. The 7 minutes beam crossing time is possible given that the GBT has ~580 km diameter beam at S-band. The crossing time also depends on the orbital geometry. The receiving beam covers the side-lobes of the transmit beam from Arecibo, although the spacecraft would have a significantly reduced SNRs if it were outside the 3 dB cone.

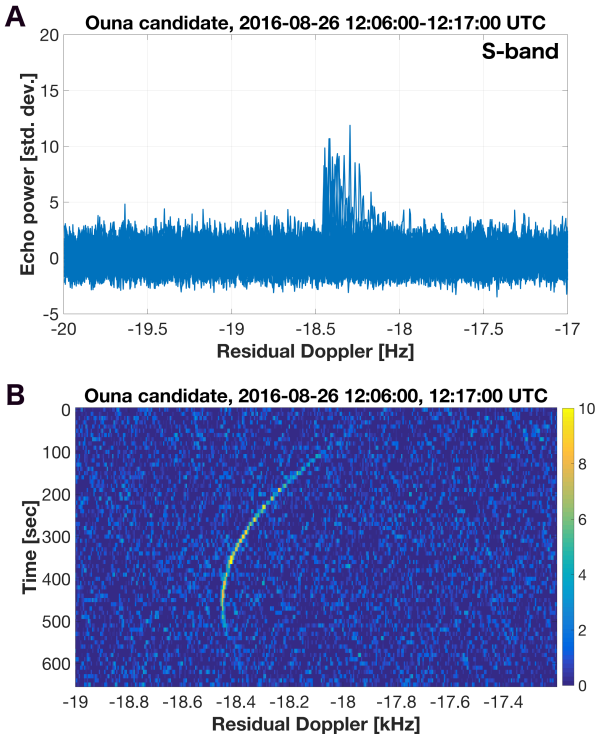


Fig. 8. Candidate Ouna detection on Aug. 26 from Arecibo and the GBT. (A) Echo power strength (in units of standard deviations above the noise level) with respect to uncompensated lunar Doppler frequencies. (B) Echo power strength in time and Doppler frequencies.

At 715 km, we were pointed at a significant distance from the lunar surface. We regularly observed spurious lunar surface echoes while pointed closer to the Moon, but the data obtained while pointed at 715 km appeared relatively clean. Hence, we were encouraged about the possibility that we have detected Ouna as opposed to a lunar glint.

The last observations scheduled for September 23 from DSS-14 and Arecibo were hampered by the power outage in Puerto Rico and associated equipment issues. No detection of

Ouna was obtained. We did search for Ouna in all previously obtained data sets, but no additional echo was found. With a single detection, there can be no certain claim about Ouna recovery, and further observations are needed.

## 4. Conclusions

Radar provides a powerful technique to track meter(s)-size spacecraft orbiting the Moon. These objects are too small and too close to the bright lunar surface to be observed optically. Goldstone's DSS-14 and Arecibo are currently the only radars in the world with lunar spacecraft tracking capabilities. The Green Bank Telescope is an ideal facility to receive the transmissions because it is a fully steerable 100-m diameter antenna. Radar observations do not depend on the time of day as long as the Moon is up on the sky. Similarly, radar can observe in a cloudy and rainy weather.

Radar observations have a pre-requisite that the plane of sky orbital uncertainties need to be smaller than the antennas beam widths which cover about a few hundred kilometers at one lunar distance. Observations must also be made at a point where the angular separation between the spacecraft and lunar surface is at least several tens of km. Otherwise strong lunar glints can mask the weak spacecraft echo. Radar astrometry puts strong orbital constraints because it allows the line of sight velocity to be measured at a precision of several cm/s. Radar can also be used to obtain ranging measurements with resolution of several tens of meters.

## Acknowledgments

In addition to the authors listed in this paper, the team consisted of: Lawrence G. Snedeker, Clement G. Lee, Kenneth S. Andrews, Zahi B. Tarzi, Philip J. Perillat, Robert Fogg, Travis W. Tennyson, Marc A. Silva, Ralph B. Roncoli, Joseph R. Guinn, Shantanu P. Naidu, and Lance A. M. Benner. We thank the Goldstone, GBT, and Arecibo technical and support staffs for help with the radar observations. This work was performed at the Jet Propulsion Laboratory, California Institute of Technology, under contract with the National Aeronautics and Space Administration (NASA).

## References

1) Ostro, S.J.: Planetary radar astronomy, *Reviews of Modern Physics* **65** (1993), pp. 1235-1279.
2) Magri, C., Nolan, M.C., Ostro, S.J. and Giorgini, J.D.: A radar survey of main-belt asteroids: Arecibo observations of 55 objects during 1999-2003. *Icarus* **186** (2007), pp. 126-151.
3) Benner, L.A.M., Busch, M.W., Giorgini, J.D., Taylor, P.A. and Margot, J.L.: Radar observations of near-Earth and main-belt asteroids, *Asteroids IV, Michel, P., DeMeo, F.E., and Bottke, W.F. (eds.)*, Univ. of Arizona Press, Tucson, USA, 2015, pp.165-182.
4) Harmon, J.K., Nolan, M.C., Ostro, S.J. and Campbell, D.B.: Radar studies of nuclei and grain comae. *Comets II*, *Festou, M.C., Keller, H.U., and Weaver, H.A. (eds.)*, Univ. of Arizona Press, Tucson, USA, 2004, pp. 265-279.
5) Harmon, J.K., Slade, M.A., Vèlez, R.A., Crespo, A., Dryer, M.J. and Johnson, J.M.: Radar mapping of Mercury's polar anomalies, *Nature* **369**, (1994), pp 213-215.
6) Slade, M.A., Zohar, S. and Jurgens, R.F.: Venus: improves spin vector from Goldstone radar observations, *Astron. J.* **100**, (1990), pp. 1369-1374.
7) Simpson, R.A. and Tyler, G.L.: Arecibo radar observations of Martian surface characteristics near the equator, *Icarus* **33**, (1978), pp. 102-115.
8) Harmon, J.K, Ostro, S.J., Chandler, J.F. and Hudson, R.S.: Radar ranging to Ganymede and Callisto, *Astron. J.* **107**, (1994), pp. 1175-1181.
9) Nicholson, P.D., French, R.G., Campbell, D.B., Margot, J.L., Nolan, M.C., Black, G.J. and Salo, H.J.: Radar imaging of Saturn's rings, *Icarus* **177**, (2005), pp. 32-62.
10) Radio astronomers find a lost satellite, https://science.nasa.gov/science-news/science-at-nasa/1998/ast28jul98_1
11) JPL's Chandrayaan-1 orbital solution post 2009 and before any radar observations (analysis by Eunice K. Lao): spk_ch1_151201_170101_150602_jpl-ekl_SCID-86.bsp, http://ssd.jpl.nasa.gov/horizons.cgi (accessed July 1, 2016).
12) JPL's Ouna orbital solution (analysis by Eunice K. Lao): ouna_071012_200101_150608_SMM0710031456-jpl-ekl.bsp, http://ssd.jpl.nasa.gov/horizons.cgi (accessed July 1, 2016).
13) Naidu, S.P., Benner, L.A.M., Margot, J.L., Busch, M.W. and Taylor, P.A.: Capabilities of Earth-based radar facilities for near-Earth asteroid observations, *Astron. J.* **152**, (2016), 99 (9pp).
14) Black, G.J.: Planetary radar astronomy in Single-Dish Radio Astronomy, *Techniques and applications ASP Conference Series*, *Stanimirovic S., Altschuler, D.R., Goldsmith, P.F., and Salter, C.J. (eds.)*, Astronomical Society of the Pacific, San Francisco, USA, 2002, pp. 271-290.
15) Magri, C., Ostro, S.J., Scheeres, D.J., Nolan, M.C., Giorgini, J.D., Benner, L.A.M. and Margot, J-.L.: Radar observations and a physical model of asteroid 1580 Betulia, *Icarus* **186**, (2007), pp. 152-177.
16) Harmon, J.K.: Planetary delay-Doppler radar and the long-code method, *IEEE Trans. Geosci. and Remote Sens.* **40**, (2002), pp. 1904-1916.
17) Smith, J.: Monte for orbit determinations. Proceedings of the ISTS Issue of Japan Society for Aeronautical and Space Science (JSASS) On-line Journal, Jun. 2017.
18) Park, R.S., Konopliv, A.S., Asmar, S.W., Bills, B. G., Gaskell, R.W., Raymond, C.A., Smith, D.E. and Zuber, M.T.: Gravity field expansion in ellipsoidal harmonic and polyhedral internal representations applied to Vesta, *Icarus* **240**, (2014), pp. 118-132.
19) Park, R.S., Konopliv, A.S., Bills, B.G., Rambaux, N., Castillo-Rogez, J.C., Raymond, C.A., Vaughan, A.T., Ermakov, A.I., Zuber, M.T., Fu, R.R., Toplis, M.J., Russell, C.T., Nathues, A., and Preusker, A.: A partially differentiated interior for Ceres deduced from its gravity field and shape, *Nature* **537**, (2016), pp. 515-517.
20) Park, R.S., Asmar, S.W., Fahnestock, E.G., Konopliv, A.S., Lu, W., and Watkins, M.M.: Gravity Recovery and Interior Laboratory Simulations of Static and Temporal Gravity Field, *Journal of Spacecraft and Rockets* **49**, (2012), pp. 390-400.
21) Folkner, W.M., Williams, J.G., Boggs, D.H., Park, R.S., and Kuchynka, P.: The Planetary and Lunar Ephemerides DE430 and DE431, *IPN Progress Report*, (2014), pp. 42-196.
22) Konopliv, A.S., Park, R.S., Yuan, D.-N., Asmar, S.W., Watkins, M.M., Williams, J.G., Fahnestock, E.G., Kruizinga, G., Paik, M., Strekalov, D., Harvey, N., Smith, D.E., an Zuber, M.T.: High-resolution lunar gravity fields from the GRAIL primary and extended missions, *Geophy. Res. Lett.* **41**, (2014), pp. 1452-1458.